Nano Research

ISSN 1998-0124 CN 11-5974/O4
https://doi.org/10.1007/s12274-023-5758-z

Research Article

Ambipolar tribotronic transistor of $MoTe_2$

Yonghai Li[1,2], Jinran Yu[2,3], Yichen Wei[1,2], Yifei Wang[2,3], Liuqi Cheng[2,4], Zhenyu Feng[2,4], Ya Yang[2,3,4], Zhong Lin Wang[2,5] (✉), and Qijun Sun[2,3,4] (✉)

[1] *Center on Nanoenergy Research, School of Chemistry and Chemical Engineering, Guangxi University, Nanning 530004, China*
[2] *Beijing Institute of Nanoenergy and Nanosystems, Chinese Academy of Sciences, Beijing 101400, China*
[3] *School of Nanoscience and Technology, University of Chinese Academy of Sciences, Beijing 100049, China*
[4] *Center on Nanoenergy Research, School of Physical Science and Technology, Guangxi University, Nanning 530004, China*
[5] *Georgia Institute of Technology, Atlanta, GA 30332-0245, USA*

Received: 31 January 2023 / **Revised:** 9 April 2023 / **Accepted:** 18 April 2023

ABSTRACT

Two-dimensional (2D) tribotronic devices have been successfully involved in electromechanical modulation for channel conductance and applied in intelligent sensing system, touch screen, and logic gates. Ambipolar transistors and corresponding complementary inverters based on one type of semiconductors are highly promising due to the facile fabrication process and readily tunable polarity. Here, we demonstrate an ambipolar tribotronic transistor of molybdenum ditelluride ($MoTe_2$), which shows typical ambipolar transport properties modulated by triboelectric potential. It is comprised of a $MoTe_2$ transistor and a lateral sliding triboelectric nanogenerator (TENG). The induced triboelectric potential by Maxwell's displacement current (a driving force for TENG) can readily modulate the transport properties of both electrons and holes in $MoTe_2$ channel and effectively drive the transistor. High performance tribotronic properties have been achieved, including low cutoff current below 1 pA·μm^{-1} and high current on/off ratio of ~ 10^3 for holes and electrons dominated transports. The working mechanism on how to achieve tribotronic ambipolarity is discussed in detail. A complementary tribotronic inverter based on single flake of $MoTe_2$ is also demonstrated with low power consumption and high stability. This work presents an active approach to efficiently modulate semiconductor devices and logic circuits based on 2D materials through external mechanical signal, which has great potential in human–machine interaction, intelligent sensor, and other wearable devices.

KEYWORDS

ambipolar, tribotronic transistor, triboelectric potential, mechanical displacement, logic gate

1 Introduction

Over the past decade, the nanofabrication techniques have been rapidly developed and facilitated the prosperity of micro/nano-devices [1]. Meanwhile, there is a growing demand for low-power electronic devices and logic circuits with the rise and rapid development of the Internet of Things (IoT) applications [2]. Recently emerging two-dimensional (2D) layered materials with outstanding optoelectronic and electronic properties have been extensively studied since the emergence of graphene in 2004 [3–8]. One reason for 2D materials attracting considerable attention is that they have shown unique properties for fundamental research and technological applications. More importantly, the field-effect transistors (FETs) based on 2D materials exhibit steep subthreshold swing, high current on/off ratio, and small off-state current, which are highly promising for low-power electronics and have great potential to break through the bottleneck of Moore's law [9–13]. As one of the typical 2D materials, transition-metal dichalcogenides (TMDs) have attached lots of interests from researchers. The adjacent layers of TMDs are assembled together by van der Waals (vdW) force [13, 14], from which the monolayer material can be easily obtained from the bulk materials to construct FETs with atomic thin channel, low-power consumption, and multifunctionality [15]. Since triboelectric nanogenerator (TENG) was invented in 2012 [16–18], tribotronic transistor, a novel device which couples triboelectric potential with FET to control/tune the charge carrier transport at the electrical contacts/junctions [19–22], can effectively replace the gate input and further reduce the power consumption [23]. Moreover, tribotronic transistors link the external stimulation with device output, realizing the active and direct detection on mechanical displacement or external force [24, 25]. 2D tribotronic devices have been successfully involved in electromechanical modulation in logic devices [12, 23], intelligent sensing system [24, 26], touch screen [27], smart switch [28], phototransistors [29], memory [30], etc. Thereinto, tribotronic logic gates based on complementary metal-oxide-semiconductor (CMOS) inverter have the advantages of lower power consumption and larger noise margins in contrast to the resistive load inverters [31, 32]. Accordingly, ambipolar tribotronic transistors and corresponding complementary inverters based on one type of semiconductors are highly promising due to the facile fabrication process and readily tunable polarity.

In 2D transistor devices, the dominant charge carrier (electron or hole in the channel) determines the channel conduction and polarity type [33]. When TMDs are used for CMOS circuits, the

Address correspondence to Qijun Sun, sunqijun@binn.cas.cn; Zhong Lin Wang, zhong.wang@mse.gatech.edu

transistor polarity can be modulated to p- (or n-) type [34, 35]. However, it is difficult to modulate the transistor polarity because of the Fermi level pinning effect [33, 36]. For instance, although the widely used MoS_2 FETs are promising due to their low off-state current [37], high electron mobility [38], and steep subthreshold swing [39], p-type MoS_2 FETs are still difficult to achieve because of the Fermi level pinning at the interface of metal–MoS_2 [40]. Many efforts have been done to overcome the Fermi level pinning phenomenon that occurs in some TMDs, e.g., work function engineering [40], chemical doping [41], and vdW contacts [42]. On the other hand, 2D ambipolar semiconductors have been intensively studied and attracted much attention. The major charge carriers in 2D ambipolar semiconductors can be dynamically, reversibly, and rapidly tuned between holes and electrons by electrostatic field [43–46]. Among various 2D ambipolar semiconductors, molybdenum ditelluride ($MoTe_2$) is receiving increasing attention due to its rich crystalline phases, superior semiconducting/metallic/superconducting properties, and attractive ambipolar properties [47–49]. Until now, ambipolar tribotronic transistors by coupling $MoTe_2$ transistor and TENG have rarely been investigated.

In this work, we present an ambipolar tribotronic transistor of $MoTe_2$, which shows typical ambipolar transport properties modulated by triboelectric potential. The presented ambipolar tribotronic device is comprised of a $MoTe_2$ FET and a lateral sliding TENG. The induced triboelectric potential by Maxwell's displacement current (a driving force for TENG) can readily modulate the transport properties of both electrons and holes in $MoTe_2$ channel and effectively drive the transistor. High performance tribotronic properties have been achieved, e.g., low cutoff current below 1 pA·μm^{-1}, and high current on/off ratio of $> 10^2$ and 10^3 for holes and electrons dominated transports, respectively. The working mechanism of realizing tribotronic ambipolarity is also discussed in detail. Furthermore, a complementary tribotronic inverter based on single flake of $MoTe_2$ was prepared, exhibiting low power consumption and high stability properties. The demonstrated ambipolar tribotronic transistor offers an active and efficient way to modulate channel conduction and polarity type through external mechanical displacement, which has shown great potential in tunable semiconductor devices, interactive logic gates, intelligent sensors, and self-powered logic systems.

2 Results and discussion

Figure 1(a) shows the schematic illustration of the ambipolar tribotronic transistor of $MoTe_2$, which is composed of integrated $MoTe_2$ FET and lateral-sliding-mode TENG component. The sliding-mode TENG component is comprised of one polytetrafluoroethylene (PTFE) film as the electronegative friction layer (attached with an Al conducting electrode) sliding against the other electronegative Al friction layer (attached to the bottom of a Si/SiO_2 wafer). The mechanical sliding between the two friction layers can lead to a relative displacement, which will induce unneutralized electrostatic charges and corresponding triboelectric potential coupled to the integrated $MoTe_2$ FET. The sliding triboelectrification induced polarization is the origin of displacement current, i.e., a time-dependent variable voltage. The $MoTe_2$ FET was prepared on the Si/SiO_2 wafer (300 nm thick SiO_2) with Cr/Au (12 nm/40 nm) as the source-drain electrodes defined by standard e-beam lithography (EBL) and electron-beam deposition. The $MoTe_2$ channel was prepared by mechanical exfoliation prior to the source-drain electrodes deposition. The channel width and length of transistor are defined to be 2 and 3 μm, respectively (top-view optical image of $MoTe_2$ transistor in Fig. S1(a) in the Electronic Supplementary Material (ESM)). The inset of Fig. 1(a) shows the enlarged hexagonal structure of $MoTe_2$, consisting of a hexagonal transition metal layer sandwiched between two chalcogen layers. Figure 1(b) shows the Raman shift of multilayer $MoTe_2$ flakes. The Raman spectrum of $MoTe_2$ exhibits the characteristic peaks nearly located at ~ 171, 234, and 289 cm^{-1}, corresponding to the three different vibration modes A_g, E_{2g}, and B_{2g} in $MoTe_2$ crystal lattice. These Raman features are in good agreement with previous reports [50, 51], and identify the channel materials as 2H-$MoTe_2$.

Prior to investigating the electrical performance of the ambipolar tribotronic transistor, the integrated components were tested at first. The transfer characteristics of the $MoTe_2$ transistor in both linear (dash line) and logarithmic scales (circle line) are illustrated in Fig. 1(c), in which typical ambipolar transport

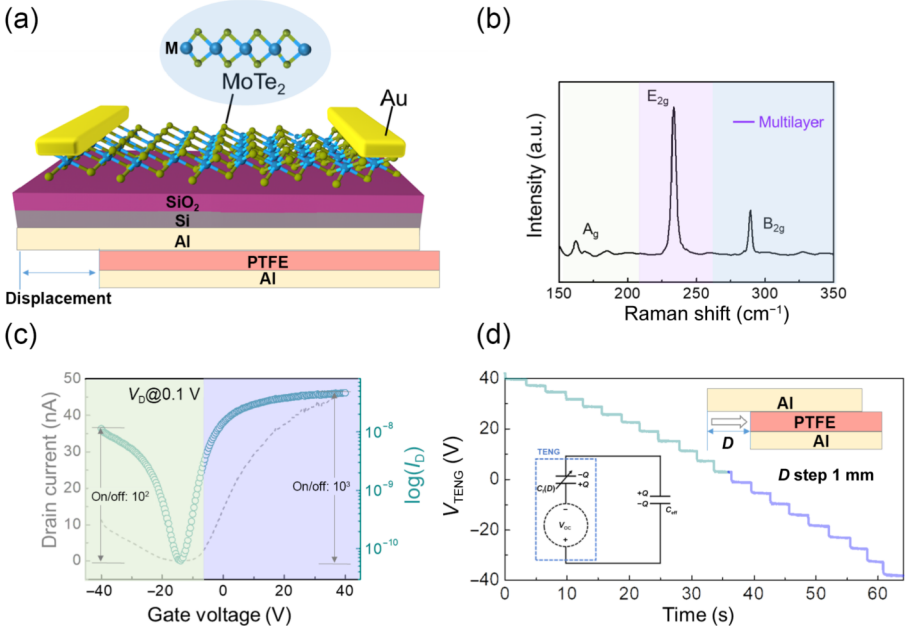

Figure 1 (a) Schematic illustration of the tribotronic transistor of $MoTe_2$. Top inset: enlarged structure of $MoTe_2$. (b) Raman shift of few-layer $MoTe_2$ flakes. (c) Typical transfer characteristics curves of the $MoTe_2$ transistor. (d) TENG output voltage (equivalent to the applied V_G) from –40 to 40 V according to one periodic displacement.

behaviors of 2H-$MoTe_2$ transistor can be observed. Under a small drain voltage (V_D) of 0.1 V, the off-state drain current (I_D) can be cut off as low as 61.7 pA at the applied gate voltage (V_G) of −7.2 V. When V_G increases from −7.2 to 40 V, I_D increases from 0.0617 to 43.7 nA, exhibiting excellent electrons-dominated transport behavior with a high on/off ratio of 10^3. When V_G decreases from −7.2 to −40 V (holes-dominated transport region), I_D also shows an increment tendency from 0.0617 to 11.3 nA with a similar on/off ratio of 10^2, indicating the intrinsic ambipolar transport behaviors of $MoTe_2$. The I_D in positive V_G region is slightly higher than that in the negative V_G region, which may be attributed to that the Schottky barrier height (SBH, φ_{BN}) for electrons is lower than that for holes. Under a dual-direction anticlockwise V_G sweeping, the transfer curves show a small hysteresis of 9.8 V (Fig. S1(b) in the ESM), indicating few defects at the interface of $MoTe_2$ and SiO_2 insulating layer. The threshold voltages (V_{TH}) are extracted from the intersections between the y-axis and reverse extension line of transfer curves in the linear region, estimating to be −19 and −7 V for holes-dominated and electrons-dominated transport regions, respectively (Figs. S1(c) and S1(d) in the ESM). The field effect mobilities for holes and electrons are evaluated to be 0.57 and 2.62 $cm^2 \cdot V^{-1} \cdot s^{-1}$, respectively. To fully realize the ambipolar properties of $MoTe_2$ transistor driven by triboelectric potential, positive and negative triboelectric voltages need to be simultaneously achieved in the integrated TENG component. Accordingly, a preset separation distance (i.e., initial relative displacement (D_0)) between Al and PTFE friction layers should be identified to readily conduct dual-direction displacement (D) so as to enable equivalent V_G in both positive and negative values (the details will be discussed in the working mechanism part). As shown in Fig. 1(d), the sliding-mode TENG part was quantitatively analyzed by using an electrometer (Keithley 6514 system, the inset is the equivalent test circuit). Upon dual-direction mechanical sliding between the two friction layers, the output voltage of TENG (V_{TENG}) decreases from 40 to −40 V with gradual decrement of the relative displacement (from $+D$ to $-D$, stepped by 1 mm), which is sufficient to drive the ambipolar tribotronic transistor of $MoTe_2$ in high performance.

The detailed operation mechanism of the ambipolar tribotronic transistor working in flat-band state, n-type state, and p-type state is explained in Fig. 2, regarding to the mechanical displacement, triboelectrification-induced charge transfer, and corresponding energy band diagrams. By presetting a mechanical displacement D_0 between Al and PTFE friction layers as the initial state (i.e., electrostatic neutralization state after grounding the Al electrode to release the triboelectrification induced charges, there is no triboelectric potential coupled to the ambipolar transistor), the $MoTe_2$ device is in flat-band state with the holes and electrons density in $MoTe_2$ channel maintaining at the pristine value (Fig. 2(a)(I)). From the aspect of energy band diagram (Fig. 2(a)(II)), the initial contact and sliding between Al and PTFE induce partial electrons to transfer from Al friction layer to PTFE/Al film due to the relatively higher electron affinity of PTFE. The grounding operation to release the induced electrostatic charges aims to implement the charge neutralization state that no triboelectric gate voltage is applied to the $MoTe_2$ transistor (V_{TENG} = 0 V). This means that no triboelectric potential influences the $MoTe_2$ channel and its conduction band and valence band both keep in the flat-band state (Fig. 2(a)(II)). When the relative displacement between Al and PTFE friction layers increases from the initial position D_0 to a larger sliding distance (D_+), the pre-induced positive electrostatic charges on Al electrode cannot be totally neutralized by the induced electrons on the counter PTFE friction layer due to the D_+ sliding. Therefore, the positive charges are lack of restriction, transfer to the gate electrode, and induce a positive

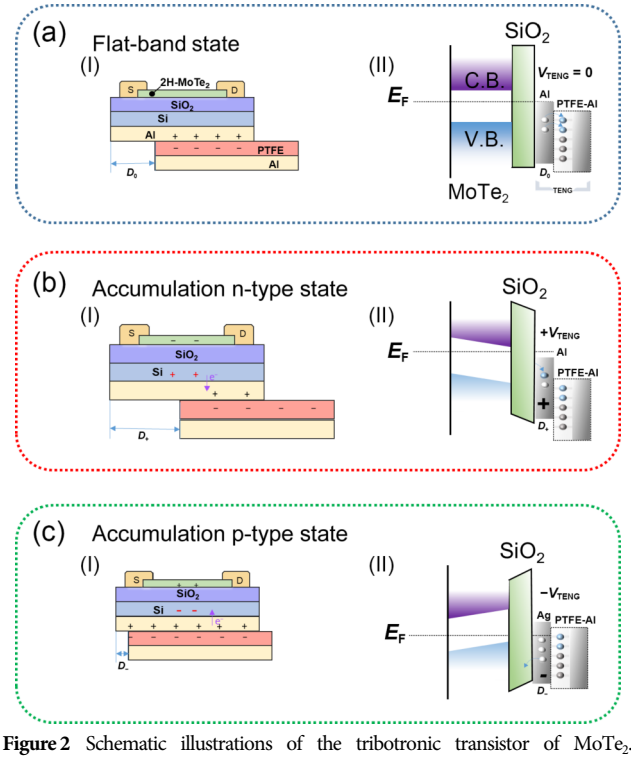

Figure 2 Schematic illustrations of the tribotronic transistor of $MoTe_2$. Working mechanism of the tribotronic transistor, explained by operation diagrams and energy band diagrams, respectively. (a) Flat-band state with a preset position of TENG component. (b) Accumulation n-type state upon positive displacement (D_+), equivalent to applying positive V_G ($+V_{TENG}$). (c) Accumulation p-type state upon negative displacement (D_-), equivalent to applying negative V_G ($-V_{TENG}$).

triboelectric potential ($+V_{TENG}$) coupled to the $MoTe_2$ channel. The coupled positive triboelectric potential is equivalent to applying a positive V_G to the $MoTe_2$ transistor, which leads to accumulated electrons in $MoTe_2$ channel to dominate the transport properties. Thus, the tribotronic $MoTe_2$ transistor works in the n-type accumulation mode (Fig. 2(b)(I)). Corresponding energy band diagram of this mode is represented in Fig. 2(b)(II). Under larger sliding displacement D_+, the unneutralized positive electrostatic charges on Al friction layer couple a positive triboelectric potential to the $MoTe_2$ channel. $+V_{TENG}$ shifts the Fermi level of $MoTe_2$ upwards and leads to the down-inclined conduction/valence band. The ambipolar tribotronic transistor of $MoTe_2$ will mainly exhibit the transport properties dominated by electrons, i.e., n-type accumulation mode. On the contrary, when the relative position between Al and PTFE friction layers decreases from the initial position D_0 to a smaller distance (D_-), more positive triboelectric charges will be attracted from transistor gate to Al friction layer and confined at the Al/PTFE sliding interface. This electrostatic induction process will result in more counter electrons left in the gate electrode and a negative triboelectric potential ($-V_{TENG}$) coupled to the $MoTe_2$ channel, equivalent to applying a negative V_G to raise the holes density in semiconductor channel. In this state, the tribotronic $MoTe_2$ transistor works in the p-type accumulation mode (Fig. 2(c)(I)). The relevant energy band diagram is presented in Fig. 2(c)(II). With Al and PTFE friction layers sliding to a smaller relative position D_-, negative triboelectric charges are induced on the gate by triboelectrification and negative triboelectric potential is coupled to the transistor channel. The $-V_{TENG}$ can shift the Fermi level of $MoTe_2$ downwards and lead to the up-inclination of conduction/valence band. In this state, holes will dominate the transport properties of the ambipolar $MoTe_2$ transistor driven by triboelectric potential, i.e., p-type accumulation mode.

The electrical characterizations of the ambipolar tribotronic transistor of $MoTe_2$ are investigated in Fig. 3. As we have mentioned above, under larger relative displacement D_+ between Al and PTFE friction layers, a positive triboelectric voltage is applied to the $MoTe_2$ transistor (Fig. 3(a)). In this state, the integrated TENG provides a positive triboelectric voltage which couples to the back gate of $MoTe_2$ transistor and induces more electrons in the channel of $MoTe_2$. With D_+ varying from 0 to 12 mm (relative to D_0), the output performances of the $MoTe_2$ tribotronic transistor are measured under the V_D bias from −1 to 1 V (Fig. 3(b)). Corresponding I_D shows an overall increment tendency under V_D in both negative and positive directions, which increases from 170 to 450 nA at V_D = −1 V and increases from 17 to 98 nA at V_D = 1 V. Corresponding tribotronic transfer characteristic curves are extracted under three specific V_D at 0.1, 0.5, and 1 V (Fig. 3(c)). At V_D = 0.1 V, I_D increases from 0.108 nA to 0.124 μA with the mechanical sliding D_+ increasing from 0 to 12 mm. At V_D = 1 V, the tribotronic transistor shows a higher current level ranging from 0.823 nA to 1.386 μA under the same mechanical displacement. The threshold displacement (D_{TH}) extracted from the intersection between reverse extension of tribotronic transfer curve and *y*-axis is evaluated to be 7 mm at the V_D bias of 0.1 V. Corresponding tribotronic mobility under triboelectric potential gating is estimated to be 0.38 $cm^2 \cdot mm^{-1} \cdot s^{-1}$. Under D_+ state with equivalently applied positive V_G, the $MoTe_2$ transistor works in n-type accumulation mode. The achieved typical output and transfer performances demonstrate the good feasibility of triboelectric potential gating under mechanical sliding action. For the situation of negative displacement D_- between Al and PTFE friction layers (Fig. 3(d)), a negative triboelectric voltage is coupled to the $MoTe_2$ transistor. With D_- changing from 0 to −18 mm (relative to D_0), the measured I_D shows almost symmetric decrement tendency under V_D in both negative and positive directions, as shown in Fig. 3(e), in which I_D decreases from 81.9 to 0.3 nA at V_D = 1 V. Notably, the measured asymmetric I_D outputs at V_D biases in opposite directions under the D_+ state (Fig. 3(b)) may be attributed to that the transport-dominated electrons in smaller size are more easily to be influenced by V_D and V_G biases compared with the holes dominated transport situation in the D_- state. For the transfer characteristics in the p-type accumulation mode extracted from Fig. 3(e), I_D changes from 6.47 to 0.11 nA with the displacement D_- changing from 0 to −18 mm at V_D = 0.1 V, representing the minimum value at D_- = −4 mm (Fig. 3(f)). The threshold displacement and the tribotronic mobility for holes transport are 14.9 mm and 0.0045 $cm^2 \cdot mm^{-1} \cdot s^{-1}$, respectively. Based on the dual-directional mechanical sliding displacement (D_+ or D_-) by the integrated TENG component, equivalent negative or positive V_G is demonstrated to be available for the tribotronic $MoTe_2$ transistor and readily drive the ambipolar transport properties, achieving ambipolar tribotronic transistor for the first time. To better understand the mechanism of the ambipolar behavior in tribotronic $MoTe_2$ transistors, band configurations of Au-$MoTe_2$ contact under different displacements are presented in Fig. 3(g). Upon the mechanical sliding displacement changed from D_- to D_+ (coupled triboelectric potential varies from negative to positive value), the $MoTe_2$ channel undergoes a significant change from p-type to n-type regime. At the preset D_0 position, there is no triboelectric potential applied to the device. The energy band of Au-$MoTe_2$ is in the pristine equilibrium state that the Schottky barrier formed at Au-$MoTe_2$ hinders the charge carriers to transport from source to drain electrode, delivering a cut-off current at ~ 10^{-10} A. When the

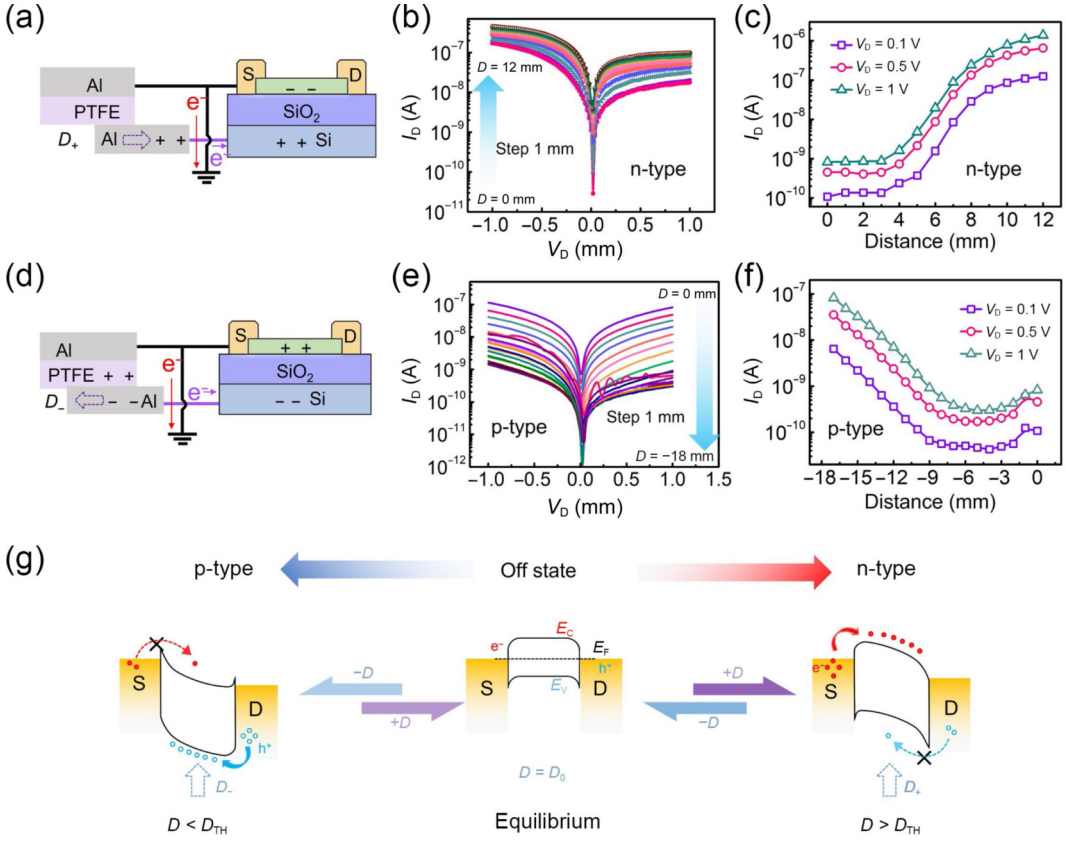

Figure 3 Electrical performance of 2H-$MoTe_2$ tribotronic transistors and the band configurations under different displacements *D*. (a) Schematic illustration of tribotronic transistor with the displacement increased from D_0 to D_+. (b) The n-type output characteristics and (c) corresponding transfer characteristics of $MoTe_2$ transistor modulated by TENG displacement. (d) Schematic illustration of tribotronic transistor with displacement decreased from D_0 to D_-. (e) The p-type output characteristics and (f) corresponding transfer characteristics of $MoTe_2$ transistor modulated by TENG displacement. (g) The band configurations under different displacements *D*.

applied mechanical displacement D increases from D_0 to D_+ until $D > D_{TH}$, the energy band is shifted downwards and up-inclined. The Schottky barrier height is reduced and electrons are injected from source to drain electrode under positive V_D bias, indicating n-type polarity of $MoTe_2$ channel. In contrast, when D changes from D_0 to D_- until $D < D_{TH}$, it can induce an equivalent negative V_G coupled to the $MoTe_2$ channel to change the transport polarity. Under the negative triboelectric potential, the energy band is shifted upwards and down-inclined. The holes will dominate the electrical properties in this state, exhibiting the p-type accumulation working mode. With the D changing to right ($D > D_{TH}$) or to left ($D < D_{TH}$), it can effectively turn the band and the Schottky barrier height. Figure S3 in the ESM shows the typical electrical performances of the fabricated pristine $MoTe_2$ transistor and corresponding band diagrams.

According to previous research [34], $MoTe_2$ has been exploited for achieving bipolar carrier conduction, which paves the way for the integration of n-type and p-type transistors to enable complementary devices. The $MoTe_2$ channel is also readily tuned by the mechanical displacement (i.e., triboelectric potential) to exhibit both p-type and n-type polarities, as demonstrated in this work. Therefore, it is feasible to combine these two methods to achieve a tribotronic complementary logic gate with one type of semiconductor material. Schematic illustration of logic gate based on two $MoTe_2$ transistors driven by electric input voltage (V_{IN}) is firstly shown in Fig. 4(a). Two $MoTe_2$ transistors are connected in series to share the common input and output terminal and driven by the applied voltage (V_{DD}, bottom circuit diagram of Fig. 4(a)). It should be noted here, in this work, the layered $MoTe_2$ exfoliated from the bulk materials tends to be n-type. In order to get the p-type $MoTe_2$, spatially controlling the doping of $MoTe_2$ channel is achieved by using photodoping method on Si/SiO_2 substrate. We choose 633 nm laser to irradiate on the pristine $MoTe_2$ to tune it into more p-type characteristics (Fig. S4 in the ESM). Figure 4(b) shows typical voltage transfer characteristics of the inverter based on the $MoTe_2$ transistors. The output voltage (V_{OUT}) coincides well with the applied V_{DD} (corresponding to the output logic "1" or "0") with the input voltage changed from −40 to 40 V (corresponding to the input logic "0" or "1"). The inverter exhibits a basic logic gate function which is qualified to implement a normative 180° phase reversal from input to output. The logic inverter displays the inversion point at −13 V, along with a logic separation of 1 V. The voltage gain expressed as gain = $-dV_{OUT}/dV_{IN}$ is extracted from the voltage transfer characteristic and evaluated to be 0.18 at a small V_{DD} of 1 V. To demonstrate the tribotronic complementary inverter based on $MoTe_2$ transistors, the mechanical displacement in the integrated TENG (to induce corresponding triboelectric potential) replaces the applied V_{IN} as the input signal. Relevant circuit diagram is shown in the bottom of Fig. 4(c). Similarly, the output voltage shows a logic reverse following the input displacement. As shown in Fig. 4(d), with the displacement D varying from −10 to 10 mm stepped by 1 mm at V_{DD} = 1 V, the V_{OUT} realizes a complete inversion from 1 V (output logic "1") to 0 V (output logic "0"). The tribotronic logic inverter displays the inversion distance at −1 mm, along with a logic separation of 0.5 V. The corresponding tribotronic gain is evaluated from the equation: gain = $-dV_{OUT}/dD$, which reaches the maximum value of 0.6 V·mm^{-1} at the logic switching distance of −1 mm.

3 Conclusions

In summary, we present an ambipolar tribotronic transistor of $MoTe_2$ modulated by triboelectric potential. The transport properties of both electrons and holes in $MoTe_2$ channel can be readily modulated by the integrated TENG displacement. High performance tribotronic properties are achieved with low cutoff current below 1 pA·μm^{-1} and high current on/off ratio of ~ 10^3 for holes and electrons dominated transports. A complementary tribotronic inverter is also demonstrated with low power consumption and high stability properties. This work demonstrates the ambipolar tribotronic transistor for the first time, presenting an active approach to efficiently modulate semiconductor devices and logic circuits for potential applications in electronic skin, intelligent sensor, and human–machine interaction.

4 Experimental

4.1 Device fabrication

All $MoTe_2$ FETs were prepared through mechanical exfoliation method from the purchased 2H-$MoTe_2$ bulk crystal and then stamp-transferred onto a Si wafer with 300 nm SiO_2 layer which

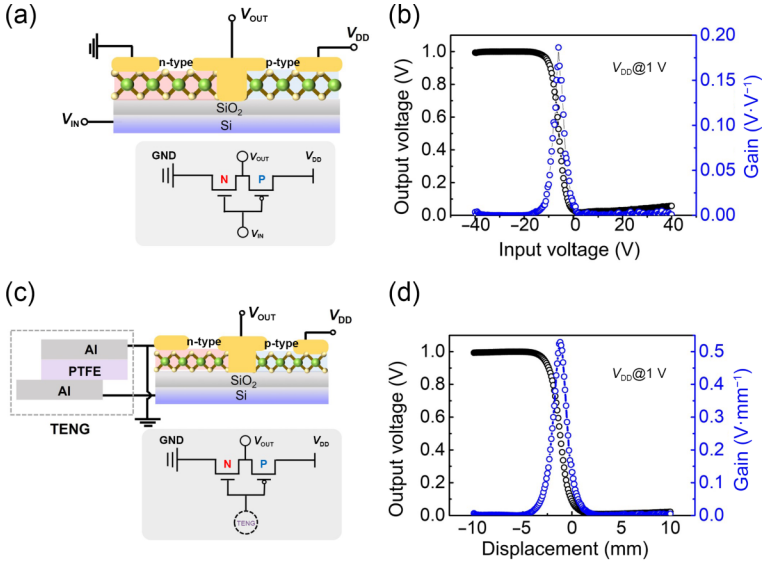

Figure 4 Electrical performance of traditional logic inverter and tribotronic logic inverter based on n-type and p-type of 2H-$MoTe_2$. (a) Schematic illustration of a typical logic inverter and its circuit schematic diagram. (b) Voltage transfer characteristic and corresponding gain value of the typical logic inverter. (c) Schematic illustration of tribotronic logic inverter and its circuit schematic diagram. (d) Voltage transfer characteristic and corresponding tribotronic gain of the ambipolar $MoTe_2$ CMOS inverter.

served as the substrate (before the transfer process, the substrates were rinsed in acetone and isopropyl alcohol). The source-drain electrodes and the bottom-gate electrode were simultaneously defined by standard EBL and thermal evaporation deposition of Cr/Au (12 nm/40 nm, respectively). To minimize the damage of the $MoTe_2$ surface and get a better contact between the electrodes and $MoTe_2$, the deposition rates were fixed at 1 Å·s^{-1} for Cr and 2 Å·s^{-1} for Au. TENG composed of an Al-PTFE-Al structure was connected to the bottom gate electrode of $MoTe_2$ FET.

4.2 Performance characterization

The electrical characterizations of the tribotronic transistors and logic devices were conducted with a semiconductor parameter analyzer (Agilent B1500A) in a probe station under ambient environment (the measurements of the electronic characteristics were performed in the dark at room temperature). The displacements of TENGs were controlled by a linear motor and the output properties of TENG were measured by Keithley 6514 system electrometer. During the test, the device and the TENG should be well screened to avoid the electrical surge from breaking down the tribotronic transistor by the surrounding electrostatic charges.

Acknowledgements

This work was financially supported by the National Key Research and Development Program of China (No. 2021YFB3200304), the National Natural Science Foundation of China (No. 52073031), the Beijing Nova Program (Nos. Z191100001119047 and Z211100002121148), the Fundamental Research Funds for the Central Universities (No. E0EG6801X2), and the "Hundred Talents Program" of the Chinese Academy of Sciences.

Electronic Supplementary Material: Supplementary material (the typical characteristics of the $MoTe_2$ transistor and the characteristics of the $MoTe_2$ transistor after laser irradiation) is available in the online version of this article at https://doi.org/10.1007/s12274-023-5758-z.

References

[1] Yang, S. H.; Lin, C. Y.; Chang, Y. M.; Li, M. J.; Lee, K. C.; Chen, C. F.; Yang, F. S.; Lien, C. H.; Ueno, K.; Watanabe, K. et al. Oxygen-sensitive layered $MoTe_2$ channels for environmental detection. *ACS Appl. Mater. Interfaces* **2019**, *11*, 47047–47053.

[2] Wang, S.; Ma, J. X.; Shi, X. Y.; Zhu, Y. Y.; Wu, Z. S. Recent status and future perspectives of ultracompact and customizable micro-supercapacitors. *Nano Res. Energy* **2022**, *1*, e9120018.

[3] Zhang, M.; Yuan, J. Y. Graphene meta-aerogels: When sculpture aesthetic meets 1D/2D composite materials. *Nano Res. Energy* **2022**, *1*, e9120035.

[4] Yu, J. R.; Yang, X. X.; Gao, G. Y.; Xiong, Y.; Wang, Y. F.; Han, J.; Chen, Y. H.; Zhang, H.; Sun, Q. J.; Wang, Z. L. Bioinspired mechano-photonic artificial synapse based on graphene/MoS_2 heterostructure. *Sci. Adv.* **2021**, *7*, eabd9117.

[5] Das, S.; Dodda, A.; Das, S. A biomimetic 2D transistor for audiomorphic computing. *Nat. Commun.* **2019**, *10*, 3450.

[6] Sun, Q. J.; Seung, W.; Kim, B. J.; Seo, S.; Kim, S. W.; Cho, J. H. Active matrix electronic skin strain sensor based on piezopotential-powered graphene transistors. *Adv. Mater.* **2015**, *27*, 3411–3417.

[7] Safaei, J.; Wang, G. X. Progress and prospects of two-dimensional materials for membrane-based osmotic power generation. *Nano Res. Energy* **2022**, *1*, e9120008.

[8] Huo, Z. W.; Yu, J. R.; Li, Y. H.; Wang, Z. L.; Sun, Q. J. 2D tribotronic transistors. *J. Phys.: Energy* **2023**, *5*, 012002.

[9] Hua, Q. L.; Gao, G. Y.; Jiang, C. S.; Yu, J. R.; Sun, J. L.; Zhang, T. P.; Gao, B.; Cheng, W. J.; Liang, R. R.; Qian, H. et al. Atomic threshold-switching enabled MoS_2 transistors towards ultralow-power electronics. *Nat. Commun.* **2020**, *11*, 6207.

[10] Liu, T.; Xiang, D.; Zheng, Y.; Wang, Y. N.; Wang, X. Y.; Wang, L.; He, J.; Liu, L.; Chen, W. Nonvolatile and programmable photodoping in $MoTe_2$ for photoresist-free complementary electronic devices. *Adv. Mater.* **2018**, *30*, 1804470.

[11] Liu, X. C.; Choi, M. S.; Hwang, E.; Yoo, W. J.; Sun, J. Fermi level pinning dependent 2D semiconductor devices: Challenges and prospects. *Adv. Mater.* **2022**, *34*, 2108425.

[12] Gao, G. Y.; Wan, B. S.; Liu, X. Q.; Sun, Q. J.; Yang, X. N.; Wang, L. F.; Pan, C. F.; Wang, Z. L. Tunable tribotronic dual-gate logic devices based on 2D MoS_2 and black phosphorus. *Adv. Mater.* **2018**, *30*, 1705088.

[13] Ma, R.; Zhang, H. R.; Yoo, Y.; Degregorio, Z. P.; Jin, L.; Golani, P.; Ghasemi Azadani, J.; Low, T.; Johns, J. E.; Bendersky, L. A. et al. $MoTe_2$ lateral homojunction field-effect transistors fabricated using flux-controlled phase engineering. *ACS Nano* **2019**, *13*, 8035–8046.

[14] Beck, M. E.; Hersam, M. C. Emerging opportunities for electrostatic control in atomically thin devices. *ACS Nano* **2020**, *14*, 6498–6518.

[15] Pezeshki, A.; Hosseini Shokouh, S. H.; Jeon, P. J.; Shackery, I.; Kim, J. S.; Oh, I. K.; Jun, S. C.; Kim, H.; Im, S. Static and dynamic performance of complementary inverters based on nanosheet α-$MoTe_2$ p-channel and MoS_2 n-channel transistors. *ACS Nano* **2016**, *10*, 1118–1125.

[16] Fan, F. R.; Tian, Z. Q.; Wang, Z. L. Flexible triboelectric generator. *Nano Energy* **2012**, *1*, 328–334.

[17] Li, Y. H.; Yu, J. R.; Wei, Y. C.; Wang, Y. F.; Feng, Z. Y.; Cheng, L. Q.; Huo, Z. W.; Lei, Y. Q.; Sun, Q. J. Recent progress in self-powered wireless sensors and systems based on TENG. *Sensors* **2023**, *23*, 1329.

[18] Dan, X. Z.; Cao, X. L.; Wang, Y. F.; Yang, J. H.; Wang, Z. L.; Sun, Q. J. A stereoscopically structured triboelectric nanogenerator for bending sensors and hierarchical interactive systems. *ACS Appl. Nano Mater.* **2023**, *6*, 3590–3598.

[19] Zhang, C.; Tang, W.; Zhang, L. M.; Han, C. B.; Wang, Z. L. Contact electrification field-effect transistor. *ACS Nano* **2014**, *8*, 8702–8709.

[20] Zhang, C.; Wang, Z. L. Tribotronics—A new field by coupling triboelectricity and semiconductor. *Nano Today* **2016**, *11*, 521–536.

[21] Yu, J. R.; Yang, X. X.; Sun, Q. J. Piezo/tribotronics toward smart flexible sensors. *Adv. Intell. Syst.* **2020**, *2*, 1900175.

[22] Yang, X. X.; Han, J.; Yu, J. R.; Chen, Y. H.; Zhang, H.; Ding, M.; Jia, C. K.; Sun, J.; Sun, Q. J.; Wang, Z. L. Versatile triboiontronic transistor via proton conductor. *ACS Nano* **2020**, *14*, 8668–8677.

[23] Gao, G. Y.; Yu, J. R.; Yang, X. X.; Pang, Y. K.; Zhao, J.; Pan, C. F.; Sun, Q. J.; Wang, Z. L. Triboiontronic transistor of MoS_2. *Adv. Mater.* **2019**, *31*, 1806905.

[24] Yang, X. X.; Yu, J. R.; Zhao, J.; Chen, Y. H.; Gao, G. Y.; Wang, Y. F.; Sun, Q. J.; Wang, Z. L. Mechanoplastic tribotronic floating-gate neuromorphic transistor. *Adv. Funct. Mater.* **2020**, *30*, 2002506.

[25] Zhang, H.; Yu, J. R.; Yang, X. X.; Gao, G. Y.; Qin, S. S.; Sun, J.; Ding, M.; Jia, C. K.; Sun, Q. J.; Wang, Z. L. Ion gel capacitively coupled tribotronic gating for multiparameter distance sensing. *ACS Nano* **2020**, *14*, 3461–3468.

[26] Yang, Z. W.; Pang, Y. K.; Zhang, L. M.; Lu, C. X.; Chen, J.; Zhou, T.; Zhang, C.; Wang, Z. L. Tribotronic transistor array as an active tactile sensing system. *ACS Nano* **2016**, *10*, 10912–10920.

[27] Khan, U.; Kim, T. H.; Ryu, H.; Seung, W.; Kim, S. W. Graphene tribotronics for electronic skin and touch screen applications. *Adv. Mater.* **2017**, *29*, 1603544.

[28] Xue, F.; Chen, L. B.; Wang, L. F.; Pang, Y. K.; Chen, J.; Zhang, C.; Wang, Z. L. MoS_2 tribotronic transistor for smart tactile switch. *Adv. Funct. Mater.* **2016**, *26*, 2104–2109.

[29] Pang, Y. K.; Xue, F.; Wang, L. F.; Chen, J.; Luo, J. J.; Jiang, T.; Zhang, C.; Wang, Z. L. Tribotronic enhanced photoresponsivity of a MoS_2 phototransistor. *Adv. Sci.* **2016**, *3*, 1500419.

[30] Li, J.; Zhang, C.; Duan, L.; Zhang, L. M.; Wang, L. D.; Dong, G. F.; Wang, Z. L. Flexible organic tribotronic transistor memory for a visible and wearable touch monitoring system. *Adv. Mater.* **2016**, *28*, 106–110.

[31] Pu, J.; Funahashi, K.; Chen, C. H.; Li, M. Y.; Li, L. J.; Takenobu, T. Highly flexible and high-performance complementary inverters of

large-area transition metal dichalcogenide monolayers. *Adv. Mater.* **2016**, *28*, 4111–4119.

[32] Cho, A. J.; Park, K. C.; Kwon, J. Y. A high-performance complementary inverter based on transition metal dichalcogenide field-effect transistors. *Nanoscale Res. Lett.* **2015**, *10*, 115.

[33] Liu, X.; Islam, A.; Guo, J.; Feng, P. X. L. Controlling polarity of $MoTe_2$ transistors for monolithic complementary logic via Schottky contact engineering. *ACS Nano* **2020**, *14*, 1457–1467.

[34] Luo, W.; Zhu, M. J.; Peng, G.; Zheng, X. M.; Miao, F.; Bai, S. X.; Zhang, X. A.; Qin, S. Q. Carrier modulation of ambipolar few-layer $MoTe_2$ transistors by MgO surface charge transfer doping. *Adv. Funct. Mater.* **2018**, *28*, 1704539.

[35] Nakaharai, S.; Yamamoto, M.; Ueno, K.; Lin, Y. F.; Li, S. L.; Tsukagoshi, K. Electrostatically reversible polarity of ambipolar α-$MoTe_2$ transistors. *ACS Nano* **2015**, *9*, 5976–5983.

[36] Yin, L.; Wang, F.; Cheng, R. Q.; Wang, Z. X.; Chu, J. W.; Wen, Y.; He, J. Van der Waals heterostructure devices with dynamically controlled conduction polarity and multifunctionality. *Adv. Funct. Mater.* **2019**, *29*, 1804897.

[37] Li, N.; Wang, Q. Q.; Shen, C.; Wei, Z.; Yu, H.; Zhao, J.; Lu, X. B.; Wang, G. L.; He, C. L.; Xie, L. et al. Large-scale flexible and transparent electronics based on monolayer molybdenum disulfide field-effect transistors. *Nat. Electron.* **2020**, *3*, 711–717.

[38] Choi, M.; Park, Y. J.; Sharma, B. K.; Bae, S. R.; Kim, S. Y.; Ahn, J. H. Flexible active-matrix organic light-emitting diode display enabled by MoS_2 thin-film transistor. *Sci. Adv.* **2018**, *4*, eaas8721.

[39] Jiang, L. W.; Dong, D. J.; Lu, Y. C. Design strategies for low temperature aqueous electrolytes. *Nano Res. Energy* **2022**, *1*, e9120003.

[40] Qu, D. S.; Liu, X. C.; Huang, M.; Lee, C.; Ahmed, F.; Kim, H.; Ruoff, R. S.; Hone, J.; Yoo, W. J. Carrier-type modulation and mobility improvement of thin $MoTe_2$. *Adv. Mater.* **2017**, *29*, 1606433.

[41] Zhang, S. Y.; Le, S. T.; Richter, C. A.; Hacker, C. A. Improved contacts to p-type MoS_2 transistors by charge-transfer doping and contact engineering. *Appl. Phys. Lett.* **2019**, *115*, 073106.

[42] Bai, Y. C.; Sun, L. X.; Yu, Q. M.; Lei, Y.; Liu, B. L. Biomolecule capturing and sensing on 2D transition metal dichalcogenide canvas. *Nano Res. Energy* **2023**, *2*, e9120043.

[43] Li, M. J.; Lin, C. Y.; Chang, Y. M.; Yang, S. H.; Lee, M. P.; Chen, C. F.; Lee, K. C.; Yang, F. S.; Chou, Y.; Lin, Y. C. et al. Facile and reversible carrier-type manipulation of layered $MoTe_2$ toward long-term stable electronics. *ACS Appl. Mater. Interfaces* **2020**, *12*, 42918–42924.

[44] Bandyopadhyay, A. S.; Saenz, G. A.; Kaul, A. B. Role of metal contacts and effect of annealing in high performance 2D WSe_2 field-effect transistors. *Surf. Coat. Technol.* **2020**, *381*, 125084.

[45] Wei, N.; Laiho, P.; Khan, A. T.; Hussain, A.; Lyuleeva, A.; Ahmed, S.; Zhang, Q.; Liao, Y. P.; Tian, Y.; Ding, E. X. et al. Fast and ultraclean approach for measuring the transport properties of carbon nanotubes. *Adv. Funct. Mater.* **2020**, *30*, 1907150.

[46] Waldrip, M.; Jurchescu, O. D.; Gundlach, D. J.; Bittle, E. G. Contact resistance in organic field-effect transistors: Conquering the barrier. *Adv. Funct. Mater.* **2020**, *30*, 1904576.

[47] Hatayama, S.; Saito, Y.; Makino, K.; Uchida, N.; Shuang, Y.; Mori, S.; Sutou, Y.; Krbal, M.; Fons, P. Phase control of sputter-grown large-area $MoTe_2$ films by preferential sublimation of Te: Amorphous, 1T', and 2H phases. *J. Mater. Chem. C* **2022**, *10*, 10627–10635.

[48] Zhou, J. Y.; Lin, Z. Y.; Ren, H. Y.; Duan, X. D.; Shakir, I.; Huang, Y.; Duan, X. F. Layered intercalation materials. *Adv. Mater.* **2021**, *33*, 2004557.

[49] He, Q. Y.; Li, P. J.; Wu, Z. H.; Yuan, B.; Luo, Z. T.; Yang, W. L.; Liu, J.; Cao, G. Q.; Zhang, W. F.; Shen, Y. L. et al. Molecular beam epitaxy scalable growth of wafer-scale continuous semiconducting monolayer $MoTe_2$ on inert amorphous dielectrics. *Adv. Mater.* **2019**, *31*, 1901578.

[50] Zhou, L.; Xu, K.; Zubair, A.; Liao, A. D.; Fang, W. J.; Ouyang, F. P.; Lee, Y. H.; Ueno, K.; Saito, R.; Palacios, T. et al. Large-area synthesis of high-quality uniform few-layer $MoTe_2$. *J. Am. Chem. Soc.* **2015**, *137*, 11892–11895.

[51] Cho, S.; Kim, S.; Kim, J. H.; Zhao, J.; Seok, J.; Keum, D. H.; Baik, J.; Choe, D. H.; Chang, K. J.; Suenaga, K. et al. Phase patterning for ohmic homojunction contact in $MoTe_2$. *Science* **2015**, *349*, 625–628.